Critically Sampled Wavelets with Composite Dilations

Glenn R. Easley* and Demetrio Labate

Abstract—Wavelets with composite dilations provide a general framework for the construction of waveforms defined not only at various scales and locations, as traditional wavelets, but also at various orientations and with different scaling factors in each coordinate. As a result, they are useful to analyze the geometric information which often dominate multidimensional data much more efficiently than traditional wavelets. The shearlet system, for example, is a particular well-known realization of this framework which provides optimally sparse representations of images with edges. In this work, we further investigate the constructions derived from this approach to develop critically sampled wavelets with composite dilations for the purpose of image coding. Not only we show that the many nonredundant directional constructions recently introduced in the literature can be derived within this setting. We also introduce new critically sampled discrete transforms which achieve much better non-linear approximation rates than traditional discrete wavelet transforms, and outperform the other critically sampled multiscale transforms recently proposed.

Index Terms— Contourlets, directional filter banks, image coding, nonlinear approximations, shearlets, wavelets

I. INTRODUCTION

Several successful methods were recently introduced in the literature to overcome the limitations of traditional separable wavelets. Indeed, while 1D wavelets are optimal at approximating point singularities, their 2D separable counterparts, which are obtained by taking tensor products of 1D wavelets, are not very efficient at processing geometric information and, as a result, are not as effective at approximating singularities along curves (e.g., edges in images). This limitation was already observed in early papers from the filter bank literature, such as [1], [2], [3], where it was first recognized the need to better deal with directional information and the importance of directional sensitivity to more effectively process image features such edges [4]. More recently, spurred by remarkable advances in computational harmonic analysis, new and more sophisticated variants of the wavelet approach were introduced, which combine multiscale analysis and directional filtering in a way which is specifically designed to handle multidimensional data with (near) optimal efficiency. The most notable of these constructions, in dimension $n = 2$, are the *curvelets* [5], the *contourlets* [6] and the *shearlets* [7], which are obtained by defining systems of analyzing

waveforms ranging not only at various scales and locations, like traditional wavelets, but also at various orientations, with the number of orientations increasing at finer scales. Thanks to their localization, anisotropy and directional properties, these systems provide near optimally sparse representations for images containing edges [8], [6], [9], which makes their applications highly competitive in imaging problems such denoising, edge detection and feature extraction, deconvolution and image separation [10], [11], [5], [12].

However, all these recent directional variants of wavelets form redundant systems (specifically, Parseval frames) rather than orthonormal bases. While this is not a limitation in many image processing applications (or it is even beneficial as in image denoising), redundancy is not desirable in other tasks such as image coding. Thus, a number of very interesting methods were proposed during the last few years to construct nonredundant versions of these systems [13], [14], [15], [16], [17]. All these nonredundant constructions are inspired by the contourlet transform and use an appropriate combination of subband coding and directional filtering. Similarly to contourlets, they exhibit a very rich set of directions which is useful for their approximation properties and set them apart from more traditional directional wavelets; unlike the curvelets, however, they use critically sampled filter banks. Notice that other notable nonredundant 'directional' wavelet-like systems include bandelets [18], directionlets [19], and nonredundant complex wavelets [20]. However these systems are either adaptive (i.e., bandelets), which significantly increases the computational burden, or they allow only a small number of directions, which seriously limits their flexibility and approximation properties.

In this paper, we take a more general and systematic point of view, and show that all of these newly introduced nonredundant variants of the contourlet transform can be derived and analyzed within the framework of *wavelets with composite dilations*. This approach, originally developed by the authors and their collaborators in [7], [21], [22], is a far-reaching generalization of the classical theory of affine systems (from which traditional wavelets are derived) and provides a very flexible setting for the construction of truly multidimensional wavelets (see also recent results in [23], [24], [25], [26]). The shearlets, in particular, are a special 2-dimensional realization of wavelets with composite dilations.

The approach described in this paper provides a unified theoretical setting for the analysis of essentially all known nonredundant directional multiscale systems that have recently appeared in the literature. In addition, it offers a general framework for the design and construction of novel multiscale

systems with 'any' desirable directional features, where the affine mathematical structure provides a natural transition from the continuous to the discrete setting. Thanks to these properties, the new critically sampled algorithms proposed in this paper compare very favorably against both traditional wavelets and the more advanced multiscale schemes recently proposed.

Another objective of this paper is to analyze the trade-off between sparsity and critical sampling. Shearlets, as well as curvelets and contourlets, were proved to be (nearly) optimally sparse thanks in part to the so-called *parabolic scaling*; that is, the frequency support of the analyzing elements satisfies the property that *width* $\propto$ *length*^{2} [8], [9]. Our observations will show that 'enforcing' this property in *critically sampled* discrete transforms, as frequently done in many of the proposed schemes, does not necessarily improve the algorithm performance. It turns out to be more important to understand how the magnitudes of edges are affected by directional filtering and anisotropic scaling depending on the properties of the data (see [27], [28], [12]). This is shown to be an essential element in the design of highly effective representation algorithms. Indeed, we will exploit this observation to develop a simple adaptive critically sampled discrete transform, which presents some similarities to the classical wavelet packet approach. This adaptive construction allows us to achieve a further improvement in the algorithms performance at the expense of a minor additional computational cost.

II. WAVELETS WITH COMPOSITE DILATIONS

For $y \in \mathbb{R}^2$, let T_y be the *translation operator*, defined by

$$T_y f(x) = f(x - y),$$

and, for a 2×2 invertible matrix a, let D_a be the *dilation operator*, defined by

$$D_a f(x) = |\det a|^{-1/2} f(a^{-1}x).$$

The classical *affine* or *wavelet systems* generated by $\Psi = \{\psi_1, \ldots, \psi_L\} \subset L^2(\mathbb{R}^n)$ are the collections of functions of the form

$$\mathcal{A}_A(\Psi) = \{D_a T_k \psi_m : a \in A, k \in \mathbb{Z}^2, m = 1, \ldots, L\}, \quad (1)$$

where A is a subset of the group $GL_2(\mathbb{Z})$ of 2×2 integer-valued invertible matrices. If

$$\|f\|^2 = \sum_{a \in A} \sum_{k \in \mathbb{Z}^n} |\langle f, D_a T_k \psi \rangle|^2,$$

for all $f \in L^2(\mathbb{R}^n)$, then $\mathcal{A}_A(\Psi)$ is a *Parseval frame* and Ψ is called a *multiwavelet* or, simply, a *wavelet* if $\Psi = \{\psi\}$. If, in addition, $\mathcal{A}_A(\Psi)$ is an orthonormal basis, then Ψ is an orthonormal (multi)wavelet.

The *affine systems with composite dilations*, which were originally introduced in [7], in dimensions $n = 2$ have the form

$$\mathcal{A}_{AB}(\Psi) = \{D_a D_b T_k \Psi : k \in \mathbb{Z}^2, a \in A, b \in B\},$$

where A, $B \subset GL_2(\mathbb{Z})$ and the matrices $b \in B$ satisfy $|\det b| = 1$. If $\mathcal{A}_{AB}(\Psi)$ is a Parseval frame (orthonormal

basis), then Ψ is called a *composite* or *AB-multiwavelet* (orthonormal composite wavelet). The theory of these systems generalizes the classical theory of wavelets and provides a simple and flexible framework for the construction of analyzing signals which exhibit many useful geometric features. In fact, the matrices $a \in A$ are expanding (i.e., eigenvalues are larger than one in magnitude) and are associated with the usual multiscale decomposition; by contrast, the matrices $b \in B$, which are non-expanding, produce rotations or other orthogonal transformations. As a result, one can construct composite wavelets with good time-frequency decay properties whose elements contain "long and narrow" waveforms with many locations, scales, shapes and directions. The *shearlets*, for example, are a special realization of composite wavelets which provide (nearly) optimally sparse representations for images with edges [7], [9] and were successfully employed to develop a number of image processing applications [10], [12].

Remarkably, the theory of wavelets with composite dilations extends many standard results from the classical wavelet theory (see [7], [21], [22] for a details). In particular, there are simple and general results for the constructions of composite wavelets where the generator ψ is chosen such that $\hat{\psi} = \chi_S$, where $S \subset \mathbb{R}^2$. Specifically, we have:

Theorem 1 ([21]): Let $\psi = (\chi_S)^\vee$ and suppose that $S \subset F \subset \mathbb{R}^2$, where

1) $\widehat{\mathbb{R}}^2 = \bigcup_{k \in \mathbb{Z}^2}(F + k)$;
2) $\widehat{\mathbb{R}}^2 = \bigcup_{a \in A, b \in B} S(ab)^{-1}$,

where the union is essentially disjoint and A, B are subsets of $GL_2(\mathbb{R})$. Then the composite wavelet system $\mathcal{A}_{AB}$ is a Parseval frame for $L^2(\mathbb{R}^2)$. If, in addition, $\|\psi\| = 1$, then $\mathcal{A}_{AB}$ is an ONB for $L^2(\mathbb{R}^2)$.

As for traditional wavelets, it is more difficult to construct multiscale directional systems which are also well localized. Some special new results will be given below.

A. Some Constructions

Using Theorem 1, we will now construct several examples of composite wavelets which provide the framework for a number of novel nonredundant discrete directional multiscale transforms. Notice that Constructions 2 and 3 are similar to examples in [21], whereas Construction 1 and its well-localized versions discussed later are new.
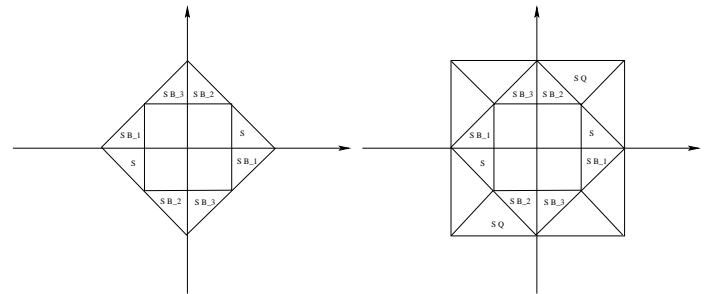

Fig. 1. *Example of composite wavelet where $a = Q$.*

1) Construction 1: Let $a = Q = \left(\begin{smallmatrix} 1 & 1 \\ -1 & 1 \end{smallmatrix}\right)$ and consider $B = \{b_0, b_1, b_2, b_3\}$ where $b_0 = \left(\begin{smallmatrix} 1 & 0 \\ 0 & 1 \end{smallmatrix}\right)$, $b_1 = \left(\begin{smallmatrix} 1 & 0 \\ 0 & -1 \end{smallmatrix}\right)$, $b_2 = \left(\begin{smallmatrix} 0 & 1 \\ 1 & 0 \end{smallmatrix}\right)$, $b_3 = \left(\begin{smallmatrix} 0 & -1 \\ -1 & 0 \end{smallmatrix}\right)$.

Let $\hat{\psi}(\xi) = \chi_S(\xi)$ where the set S is the union of the triangles with vertices $(1,0), (2,0), (1,1)$ and $(-1,0), (-2,0), (-1,-1)$ and is illustrated in Figure 1. Notice that S satisfies the assumptions of Theorem 1. Hence the system

$$\{D_a^i D_b T_k \psi : i \in \mathbb{Z}, b \in B, k \in \mathbb{Z}^2, \}$$

is an ONB for $L^2(\mathbb{R}^2)$ (in fact, it is a Parseval frame and $\|\psi\| = 1$).

Indeed, the frequency partition achieved by the Hybrid Quincunx Wavelet Directional Transform (HQWDT) from [15] is a simple modification of this construction, which is obtained by splitting each triangle of the set S into 2 smaller triangles, say, $S = S_1 \cup S_1$, so that we have the frequency tiling illustrated in Figure 2. This can be expressed as the composite wavelet system

$$\{D_a^i D_b T_k \psi^m : i \in \mathbb{Z}, b \in B, k \in \mathbb{Z}^2, m = 1, 2\},$$

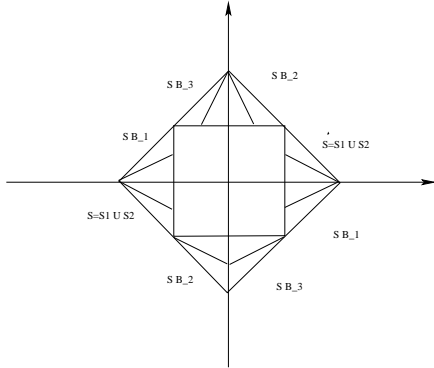where $\hat{\psi}^m(\xi) = \chi_{S_m}(\xi)$, $m = 1, 2$.

Fig. 2. *Example of composite wavelet system with $a = Q$.*

2) Construction 2: Let $a = \left(\begin{smallmatrix} 2 & 0 \\ 0 & 2 \end{smallmatrix}\right)$ and consider $B = \{b, b_1, b_2, b_3\}$ where $b_0 = \left(\begin{smallmatrix} 1 & 0 \\ 0 & 1 \end{smallmatrix}\right)$, $b_1 = \left(\begin{smallmatrix} 1 & 0 \\ 0 & -1 \end{smallmatrix}\right)$, $b_2 = \left(\begin{smallmatrix} 0 & 1 \\ 1 & 0 \end{smallmatrix}\right)$, $b_3 = \left(\begin{smallmatrix} 0 & -1 \\ -1 & 0 \end{smallmatrix}\right)$.

Let R be the union of the trapezoid with vertices $(1,0), (2,0), (1,1), (2,2)$ and the symmetric one with vertices $(-1,0), (-2,0), (-1,-1), (-2,-2)$. Next, we partition each trapezoid into equilateral triangles R_m, $m = 1, 2, 3$ as illustrated in Figure 3. Hence we define $\hat{\psi}^m(\xi) = \chi_{R_m}(\xi)$, $m = 1, 2, 3$. Then the system

$$\{D_a^i D_b T_k \psi^m : i \in \mathbb{Z}, b \in B, k \in \mathbb{Z}^2, m = 1, 2, 3\}$$

is an orthonormal basis for $L^2(\mathbb{R}^2)$.

3) Construction 3: Another example of composite wavelet system is obtained by keeping the same dilation matrix a of Example 2, and redefining B as the set $\{b^\ell : -3 \leq \ell \leq 2\}$ where b is the shear matrix $\left(\begin{smallmatrix} 1 & 1 \\ 0 & 1 \end{smallmatrix}\right)$. Then, by letting R be the union of the trapezoid with vertices $(1,0), (2,0), (1,1/3), (2,2/3)$ and the symmetric one with vertices $(-1,0), (-2,0), (-1,-1/3), (-2,-2/3)$, and
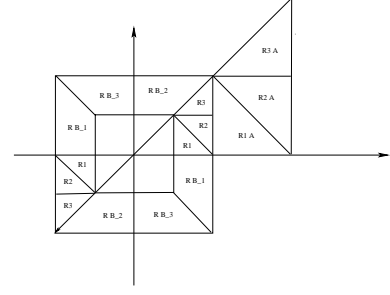

Fig. 3. *Example of composite wavelet system with $a = 2I$.*

$\hat{\psi}^m(\xi) = \chi_{R_m}(\xi)$, where $R_m = R b^m$, it follows that the system

$$\{D_a^i D_b T_k \psi^m : i \in \mathbb{Z}, b \in B, k \in \mathbb{Z}^2, m = 1, 2, 3\}$$

is an orthonormal basis for $L^2(\mathcal{D}_0) = \{f \in L^2(\mathbb{R}^2) : \text{supp} \, \hat{f} \subset \mathcal{D}_0\}$, where $\mathcal{D}_0 = \{(\omega_1, \omega_2) : |\omega_2/\omega_1| \leq 1\}$. To obtain an orthonormal basis for the whole space $L^2(\mathbb{R}^2)$, it is sufficient to add a similar system which is an orthonormal basis for $L^2(\mathcal{D}_1)$ where $\mathcal{D}_1 = \{(\omega_1, \omega_2) : |\omega_2/\omega_1| \geq 1\}$. This is given by

$$\{D_a^i D_b T_k \tilde{\psi}^m : i \in \mathbb{Z}, b \in \tilde{B}, k \in \mathbb{Z}^2, m = 1, 2, 3\},$$

where $\tilde{B} = \{(b^T)^\ell : -3 \leq \ell \leq 2\}$. Finally, the low frequency region of the spectrum is covered using a standard wavelet basis. The frequency tiling corresponding to this system is illustrated in Figure 4. This frequency tiling is
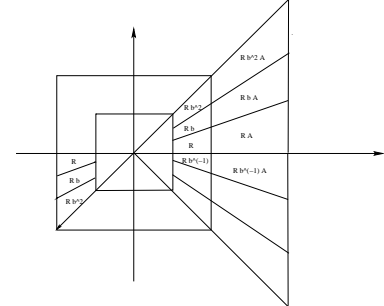

Fig. 4. *Example of composite wavelet system with $a = 2I$ and shearing matrix.*

similar to the one used for the NonUniform Directional Filter Bank (NUDFB) in [29]. If this construction is combined with a separable generator, then one obtains the frequency tiling which corresponds to the Hybrid Wavelet Directional Transform (HWDT) from [15] and to the directional filter bank construction used in [17].

4) Additional Constructions: The contourlet and shearlet systems mentioned in the introduction are also based on a frequency tiling similar to Construction 3. In these cases, however, the dilations matrix a is given by $a = \left(\begin{smallmatrix} 4 & 0 \\ 0 & 2 \end{smallmatrix}\right)$, so that the number of directional bands increases at fine scales. In particular, the shearlet approach allows one to construct a *well localized* system of functions where the generator $\hat{\psi}$ is a smooth waveform rather than the characteristic function of a set. This idea leads to the development of the Parseval frame (PF) of shearlets (for details see [9], [10]).

We will now show that also for Constructions 1 and 2 it is possible to obtain well localized versions of these systems. Specifically, using the matrices from Construction 1, let $\psi \in L^2(\mathbb{R}^2)$ be defined in the frequency domain as

$$\hat{\psi}(\xi) = \hat{\psi}(r, \theta) = V(r) \, U(\theta).$$

We assume that $V \in C^\infty(\mathbb{R})$ is compactly supported in $[0, \frac{1}{2}]$ and it satisfies

$$\sum_{i \in \mathbb{Z}} |V((\sqrt{2})^i r)|^2 = 1 \quad \text{a.e. on } [0, \infty).$$

We also assume that $U \in C^\infty([-\pi, \pi])$ is periodic, compactly supported inside $[-\pi, \pi]$ and it satisfies:

$$\sum_{\ell=0}^{3} |U(\theta + \ell\frac{\pi}{4})|^2 = 1 \quad \text{a.e. on } [-\pi, \pi].$$

Hence ψ is a well-localized function, with $\operatorname{supp} \hat{\psi} \subset [-1/2, 1/2]^2$. We then have the following result:

Theorem 2: The system

$$\{D_Q^i \, D_{b_\ell} \, T_k \, \psi : i \in \mathbb{Z}, \, \ell = 0, 1, 2, 3, \, k \in \mathbb{Z}^2\} \tag{2}$$

is a Parseval Frame for $L^2(\mathbb{R}^2)$, and an ONB if $\|\psi\| = 1$.
Proof. Notice that

$$\xi \, Q^i \, b_\ell = ((\sqrt{2})^i r, \theta + i\frac{\pi}{4} + \ell\frac{\pi}{4}),$$

where we have used the fact that $Q = \sqrt{2} \, R_{\frac{\pi}{4}}$, where $R_{\frac{\pi}{4}}$ is the rotation matrix by $\pi/4$. Hence

$$\sum_{i \in \mathbb{Z}} \sum_{\ell=0}^{3} |\hat{\psi}(\xi \, Q^i \, b_\ell)|^2$$
$$= \sum_{i \in \mathbb{Z}} \sum_{\ell=0}^{3} |\hat{\psi}(\sqrt{2})^i r, \theta + i\frac{\pi}{4} + \ell\frac{\pi}{4}|^2$$
$$= \sum_{i \in \mathbb{Z}} |V((\sqrt{2})^i r)|^2 \sum_{\ell=0}^{3} |U(\theta + (\ell+i)\frac{\pi}{4}|^2 = 1,$$

for a.e. $\xi \in \mathbb{R}^2$. Since $\operatorname{supp} \hat{\psi} \subset [-1/2, 1/2]^2$, this implies that the system (2) is a Parseval frame for $L^2(\mathbb{R}^2)$. $\square$

Notice that the elements of the system (2) are well localized waveforms whose frequency tiling corresponds approximately to Figure 1. That is, in this case, the figure illustrates the essential frequency support of the elements of this composite wavelets system, rather than their actual frequency support since their supports do overlap.

Finally, it is useful to observe that the framework of composite wavelets allows one even greater flexibility in the construction of angular subdivisions, since the matrices B in the expression (1) do not need to be of the form $\{b^\ell\}$ nor need to form a group, but can be designed as an essentially arbitrary set of (nonexpanding) matrices depending, possibly, on the resolution level. Thanks to this flexibility, it is possible to refine the directional sensitivity depending on the properties of the data and this will be especially useful for the digital implementations described below, where new critically sampled multiscale and multidirectional transforms are introduced.

III. CRITICALLY SAMPLED TRANSFORMS

We will describe how to derive discrete implementations of critically sampled directional multiscale transforms whose spatial-frequency tilings is consistent with some of the constructions described above. In particular, these implementations will take advantage of a critically sampled 2D separable discrete wavelet transform (DWT) and of a quincunx-based discrete wavelet transform (QDWT). For brevity, we will only describe in detail the construction using a critically sampled 2D separable DWT; the case of QDWT is similar and will be only sketched.

Given a 1D scaling function ϕ and a wavelet function ψ, 2D separable wavelets [30] are obtained as $\psi^1(x) = \phi(x_1)\psi(x_2)$, $\psi^2(x) = \psi(x_1)\phi(x_2)$ and $\psi^3(x) = \psi(x_1)\psi(x_2)$. As usual, let us denote as V_j and W_j the 1D approximation space and detail space determined by the 1D scaling and wavelet functions. Hence, for $p = 1, 2, 3$, the functions

$$\{\psi_{j,n}^p(x) = 2^{j/2}\psi^p(2^j x - n) : n \in \mathbb{Z}^2\}$$

determine the ON bases for the detail subspaces $V_j \otimes W_j$, $W_j \otimes V_j$, and $W_j \otimes W_j$, respectively. The 2D approximation space $V_j \otimes V_j$ is generated by $\{2^{j/2}\phi^2(2^j x - n)\}_{n \in \mathbb{Z}^2}$ where $\phi^2(x) = \phi(x_1)\phi(x_2)$.

Next, in the frequency domain, we define the functions:

$$S^{(0)}(\omega) = S_1(\omega_1)S_2(\frac{\omega_2}{\omega_1}), \quad S^{(1)}(\omega) = S_1(\omega_2)S_2(\frac{\omega_1}{\omega_2}),$$

where $S_1, S_2 \in C^\infty(\mathbb{R})$ and are compactly supported. Under appropriate assumptions on S_1, S_2 (as in the discrete shearlet construction in [10]), we can choose $\Phi \in C_0^\infty(\mathbb{R}^2)$ to satisfy

$$|\Phi(\omega)|^2 + \sum_{d=0}^{1} \sum_{j \geq 0} \sum_{\ell=-2^j}^{2^j-1} |S^{(d)}(\omega a^{-j} b_d^{-\ell})|^2 \, \chi_{\mathcal{D}_d}(\xi) = 1$$

where $b_0 = \left(\begin{smallmatrix} 1 & 1 \\ 0 & 1 \end{smallmatrix}\right)$, $b_1 = b^T$, $\omega \in \mathbb{R}^2$, $\mathcal{D}_d$ is given in Construction 3 and $\phi = (\Phi)^\vee$. Notice that each element $S^{(d)}(\omega a^{-j} b_d^{-\ell})$ is associated with a scale level j and an orientation index ℓ, according to the action of the shear matrix $b_d^{-\ell}$; the index d indicates either the mostly horizontal ($d = 0$) or the mostly vertical ($d = 1$) elements. Correspondingly, in the space domain, we have the elements $s_{j,\ell,k}^{(d)}(x) = 2^{\frac{3j}{2}} s^{(d)}(b_d^\ell a^j x - k)$, where $s^{(d)} = (S^{(d)})^\vee$. It turns out that the collection of $\{\phi(x - k) : k \in \mathbb{Z}^2\}$ together with

$$\{s_{j,\ell,k}^{(d)}(x) : j \geq 0, \, -2^j + 1 \leq \ell \leq 2^j - 2, \, k \in \mathbb{Z}^2, d = 0, 1\}$$

and

$$\{\tilde{s}_{j,\ell,k}^{(d)}(x) : j \geq 0, \, \ell = -2^j, 2^j - 1, \, k \in \mathbb{Z}^2, d = 0, 1\},$$

is a Parseval frame for $L^2(\mathbb{R}^2)$. Notice that the last set, where $\tilde{S}_{j,\ell,k}^{(d)} = S_{j,\ell,k}^{(d)} \chi_{\mathcal{D}_d}$, is needed to take care of the corner elements [10].

To obtain a directional decomposition of the 2D detail subspaces at each level $j \geq 0$ we proceed as follows. For each $p = 1, 2, 3$ (corresponding to the detail subspaces $V_j \otimes W_j$, $W_j \otimes V_j$, and $W_j \otimes W_j$, respectively) and $d = 0, 1$, we define the functions

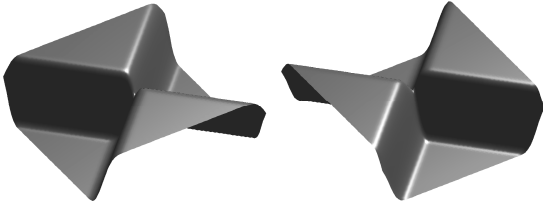$$\nu_{j,\ell_p,k}^{(d)}(x) = \sum_{k'} s_{j,\ell_p,k-k'}^{(d)}(x) \, \psi_{j,k'}^p(x),$$

Fig. 5. Spatial-frequency response of the pair of Meyer-based fan filters used in the DWTShear tranform.

where $k \in \mathbb{Z}^2$ and $-2^{j_p(j)} + 1 \le \ell_p \le 2^{j_p(j)} - 2$, and

$$\tilde{\nu}_{j,\ell_p,k}^{(d)}(x) = \sum_{k'} \tilde{s}_{j,\ell_p,k-k'}^{(d)}(x)\, \psi_{j,k'}^p(x),$$

where $k \in \mathbb{Z}^2$ and $\ell_p = -2^{j_p(j)}, 2^{j_p(j)} - 1$. Notice that the orientation index ℓ_p depends both on the scale index j and the detail subspace index p. These functions form the basis elements for the directional subspaces associated to each of the detail subspaces at scale level j. Since the transform based on this decomposition combines a discrete wavelet transform (DWT) and a directional filtering based on the shearlet transform, it will be referred to as the *DWTShear* transform.

Because the directional filtering component entails the use of compactly supported functions in the Fourier domain, we use a Meyer-based filtering method similar to those developed by the authors in [10], [31]. This is a key element in our approach since it guarantees an infinite number of directional vanishing moments which is important for the numerical implementation. Notice that this property was used to prove the optimality of the shearlet representation for a large class of images [9] and was demonstrated to be highly effective for the analysis and detection of edges [10], [32].

For this specific construction in the Fourier domain on an $N \times N$ grid, we explicitly design a fan filter oriented parallel to the ω_1 direction by evaluating the expression $S(\frac{\omega_2}{\omega_1})$ where S is a Meyer wavelet function. Given the prototype fan filter F_0, the companion prototype filter F_1 is created as a 90 degree rotation of F_0. The perfect reconstruction condition is then enforced by using the filters $F_0(\omega_1, \omega_2)/F(\omega_1, \omega_2)$ and $F_1(\omega_1, \omega_2)/F(\omega_1, \omega_2)$ where $F(\omega_1, \omega_2) = \sqrt{|F_0(\omega_1, \omega_2)|^2 + |F_1(\omega_1, \omega_2)|^2}$. These filters are then used to form a directional filter bank.

As similarly pointed out in [10], since the construction is independent of the image to be decomposed, there is a degree of freedom in choosing the size N of the Meyer fan filter. In particular, by increasing the support size to 128, we obtain filters with good directional properties. In comparison with the fan filter pairs created by conventional methods such as the maximally flat triple or double halfband filters suggested in [15] whose support sizes are 23×23, 45×45, and 29×29, 43×43, respectively, these Meyer-based fan filters offer better directional regularity and smoothness properties. Figure 5 provides some example images of these filters in the Fourier domain.

Since the detail subspaces of the DWT are each decomposed by a Parseval Frame, it follows that the DWTShear system is

a Parseval Frame for $L^2(\mathbb{R}^2)$:

Theorem 3: The elements $\{\nu_{j,\ell_p,k}^{(d)}(x), : j \ge 0, -2^{j_p(j)} + 1 \le \ell_p \le 2^{j_p(j)} - 2, k \in \mathbb{Z}^2, d = 0, 1, p = 1, 2, 3\}$, *together with* $\{\tilde{\nu}_{j,\ell_p,k}^{(d)}(x) : j \ge 0, k \in \mathbb{Z}^2, \ell_p = -2^{j_p}, 2^{j_p} - 1, d = 0, 1, p = 1, 2, 3\}$ *and* $\{\phi_k : k \in \mathbb{Z}^2\}$ *form a Parseval Frame for* $L^2(\mathbb{R}^2)$.

As mentioned above, using similar approach one obtains a directional transform which uses a quincunx-based discrete wavelet transform (QDWT) rather than the DWT. We will refer to this new transform which combines QDWT and the shearlet-based directional filtering as *QDWTShear*. This produces the frequency tiling described in Construction 1. A similar result to the Theorem 3 above is true for the QDWTShear system.

Another interesting variant of our composite transforms is obtained by using the NUDFB and applying our shearlet-based directional decomposition to each of the 5 directional components. This will be referred to as *CShear*, which is short for "composite-wavelet shearlet transform".
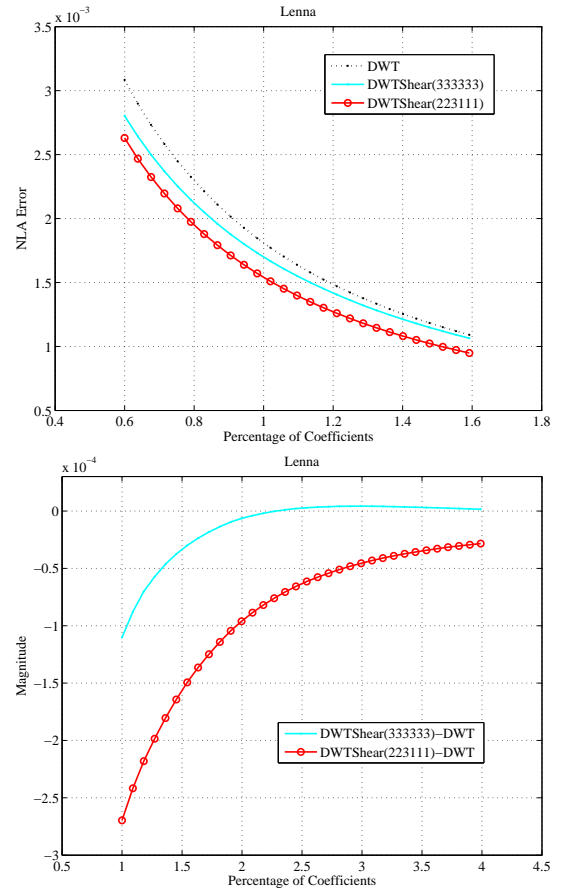

Fig. 6. The graph on top shows the errors of the nonlinear approximation (NLA) rates as functions of the percentage of coefficients used for the *Lenna* image for various transforms. Below is the difference in NLA between DWTShear(333333) and the DWT as well as the difference in NLA between DWTShear(223111) and the DWT. Notice that the data are normalized. The data illustrate the difference in performance between the new multiscale directional decompositions and the DWT, but also among versions of DWTShear with different directional decompositions. In particular, DWTShear(223111) performs better than DWTShear(333333). Observe that DWTShear(333333) follows the same directional decomposition rule as HDWT.

A. An adaptive variant

Curvelets and shearlets provide a non-adaptive method for the representation of images which achieves optimal efficiency thanks to its ability to capture the geometry of edges. To recall the heuristic idea at the core of their construction, let f be an image containing an edge along a regular curve. Using a traditional wavelet system, at scale 2^{-j}, each analyzing wavelet has essential support on a region of size $2^{-j} \times 2^{-j}$, so that it takes about 2^j wavelet coefficients to accurately represent the edge. By contrast, shearlets and curvelets have support on a region of size $2^{-j} \times 2^{-j/2}$. Since the analyzing elements are directional and only those aligned with the edge produce significant coefficients, it only takes $2^{j/2}$ such coefficients to accurately represent the edge at scale 2^{-j}. This observation indicates how directional multiscale systems with parabolic scaling are able to achieve sparser image representations. One should also notice, however, that curvelets and shearlets are built using a larger dictionary than wavelets. In particular, at scale 2^{-j}, for signals on $[0,1]^2$, there are 2^{2j} elements in an ON wavelet basis but about $5 \cdot 2^{2j}$ elements in a tight frame of shearlets [10]. The size of the dictionary of analyzing waveforms is necessarily reduced when non-redundancy is imposed on a representation system so that a formal enforcement of parabolic scaling does not guarantee a sparser representation. This is why we have allowed the range of the orientation index ℓ_p, at each scale level j, to depend also on the detail subspace index p.

To illustrate how the choice of the number of orientations affects performance of the DWTShear, we have tested several versions of the algorithm. For brevity of notation, we will express the special choice of directional decomposition of the DWTShear using the list $(j_1(1)j_2(1)j_3(1)j_1(2)j_2(2)j_3(2)\ldots)$, where $j_p(j)$ indicates that, at the scale level j, in the detail subspace associated with p, there are $2^{j_p(j)}$ orientations. For example, DWTShear(223111) indicates that, at the level $j=1$, there are $4,4,8$ orientations corresponding to the subspace indices $p=1,2,3$, respectively and, at the level $j=2$, there are 2 orientations in each detail subspace. An illustration of the performance of the DWTShear implementation in terms of its nonlinear approximation properties is given in Figure 6 using the *Lenna* image displayed in Figure 7, where it is compared against the discrete wavelet transform. Recall that, if $\tilde{f}_N$ is the approximation of f obtained by taking the N largest coefficients in its transform-domain decomposition, then the NonLinear Approximation error is

$$\text{NLA Error } = \|f - f_N\|_{L^2}^2.$$

The plots show that our choice of DWTShear(223111) performs better than the decomposition DWTShear(333333) which follows the same decomposition of rule of the HDWT (see [15] for details). This also illustrates the point that enforcing strict parabolic scaling in critically sampled representations does not guarantee the best approximation rate which, as we shall see, is part of the reason why the DWTShear tends to perform better than analogous suggested critically sampled transforms.

The result shown in Figure 6 is confirmed by many other examples of images which have been tested and have shown that the decomposition DWTShear(223111) performs very well in general. It is clear that the performance of the discrete transform, in terms of its nonlinear approximation properties, can be improved by selecting the parameters $j_p(j)$ adaptively. Indeed, Figure 6 clearly suggests that, in some cases, if the parameters $j_p(j)$ are not chosen appropriately, the approximation rate may be only slightly better in certain ranges of the percentage of the number of coefficients used. In particular, the graph on the bottom shows that DWTShear(333333) performs worse than the wavelet transform in terms of the approximation rate between 2.5 and 4 percent of the coefficients used.

To address this task, we have introduced an adaptive version of the multiscale directional method described above where each parameter $j_p(j)$ is sequentially increased, and the resulting Shannon-Weaver entropy function $\mathcal{E}(f) = -\sum_n |f_n|^2 \log |f_n|^2$ is tested to find the value that gives the minimal entropy. Since the $j_p(j) + 1$ decomposition of a region is computed from the $j_p(j)$ decomposition of the same region, this processes can be efficiently done and the process can be stopped once the measurements of entropy no longer decrease. This idea is clearly related to the wavelet packet basis approach [30]. At the same time, our multiscale decomposition does not follow exactly into the framework of wavelet packets. In particular, this new adaptation will produce a much simpler decomposition structure, such as a set of 6 integers indicating $j_p(j)$. For example, consider the case of a quadrant containing an angled linear segment that goes through the center of the quadrant and has an angle that is not a multiple of $\pi/2$. An adaptive angular subdivision will produce a decomposition so that one or at most two angular segments contain information regarding the linear segment whereas a wavelet packet subdivision will produce a square dyadic decomposition that contains many small dyadic squares in the vicinity of the linear segment. Additional observation about this point will be discussed in the next section.

Numerical examples of the adaptive scheme are illustrated in Figure 9. In particular, the adaptive variant of DWTShear has found a unique decomposition of *Lenna* corresponding to the fact that more edge information is located in the regions $p=1$ and $p=3$.

IV. EXPERIMENTAL RESULTS

In this section, we present extensive numerical demonstrations of our proposed algorithms and compared their nonlinear approximation (NLA) capabilities to those of the full hybrid DWT (HDWT), the full hybrid QDWT (HQDWT) [15], the non-uniform directional filter based (NUDFB), the quincunx non-uniform directional filter based (QNUDFB) [29], and the critically sampled contourlet transform (CSCT) [16]. Recall that the HDWT and the NUDFB are based on a decomposition of the frequency plane which is comparable to the DWTShear, while the HQDWT and the QNUDFB are comparable to the QDWTShear. However, as described above, our approach employs a different directional filters design derived from the shearlet transform. In addition, it uses a different (and
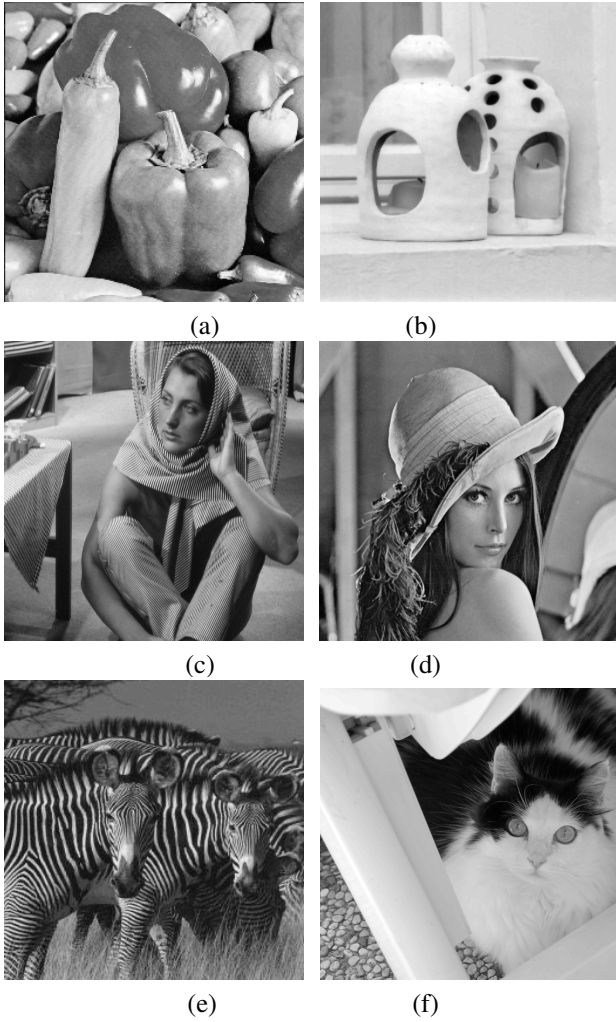
Fig. 7. Images used in this paper for different experiments. (a) *Peppers* image (512 × 512), (b) *Lamp* image (256 × 256), and (c) *Barbara* image (512 × 512), (d) *Lenna* image (1024 × 1024), (e) *Zebra* image (256 × 256), (f) *Cat* image (2000 × 2048).
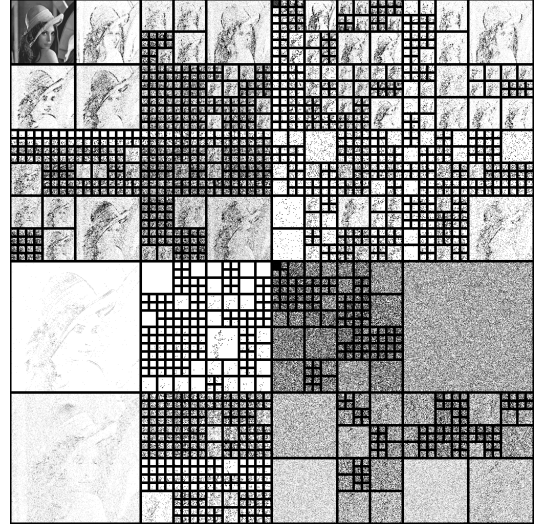

Fig. 8. An adaptive wavelet packet analysis of the Lenna image. The first two decomposition levels are broken down to 5 levels. A bit stream of length 682 is needed to store the decomposition structure.

TABLE I
PSNR VALUES OF THE NLA FOR THE LENNA IMAGE COMPARING
DWTSHEAR AGAINST WP.

| Num. of coeff. | 10625 | 11938 | 13250 | 14563 | 15875 |
	1.01%	1.14%	1.26%	1.39%	1.51%
DWPT	16.54	18.82	21.59	24.66	27.54
DWTShear(223111)	16.80	19.18	22.02	25.03	27.98
DWTShear(414113)	16.79	19.17	22.01	25.02	27.96

more flexible) strategy for choosing the number of directional bands at each resolution level. For a basic reference we also compared against the shearlet transform. Recall that the shearlet transform is a redundant transform, so that the actual percentage of coefficients used for this transform is three fourths of the percentage given in the top row of the tables.

We used the images *Peppers*, *Lamp*, *Barbara*, *Lenna*, *Zebra*, and *Cat* shown in Figure 7. In our implementations, we tested either a 3 level or 5 level decomposition of the various transforms to demonstrate the differences in performance. The DWT was implemented with the Daubechies 9/7 filters. These filters were also used for the DWT component of the DWT-Shear implementation. For the DWTShear decompositions either $j_1(1) = 2, j_2(1) = 2, j_3(1) = 3, j_1(2) = 1, j_2(2) = 1$, and $j_3(2) = 1$ were used or $j_p(j)$ were adaptively determined for $j = 1, 2$ and $p = 1, 2, 3$. In the case of QDWTShear decomposition, we set $j_p(j) = 3$ for $j = 1, 2, 3$. The CShear transform tested was with $j_p(j) = 1$ for $p = 1, \ldots, 5$ and $j = 1, 2$. The shearlet transform was implemented with angular subdivisions of $2, 4, 4$ or $2, 4, 4, 8, 8$. from coarse to fine scale depending on the number of levels tested for the particular experiment. Figure 9 illustrates some example decompositions.

For the nonadaptive DWTShear transform, we have used DWTShear(223111). In line with our discussion on the adaptive variant compared to the discrete wavelet packet transform (DWPT), we have made comparisons in terms of the approximation rates based on the number of coefficients needed to be stored (including the appropriate offsets due to the structural elements that also need to be stored). The results are given in Table IV with the wavelet packet decomposition used displayed in Figure 8. The DWTShear transforms used had same number of decomposition levels as well.

Comparison of the proposed algorithms with the other recently introduced critically sampled transforms is illustrated in Figures 10 through 12 and detailed numerical results are presented in Tables IX through VIII.

As indicated above, it turns out that, in many experiments, DWTShear(223111) achieves the best performance. This indicates that this version will be very well suited to applications where adaptive routines are prohibitive. Yet it can be observed that the adaptive variants (easily identified as having a decomposition other than 223111) in several cases improve the performance by almost a half to one decibel.

In certain ranges of the number of coefficients used for some particular images, a few of the competitive routines performed below the DWT's NLA rate, as illustrated in Figure 10. This can be understood in part by referring to Figure 6. Since the

TABLE II
PSNR VALUES OF THE NLA FOR THE PEPPERS IMAGE.

Num. of coeff.	5225 1.99%	5669 2.16%	6113 2.33%	6557 2.50%	7000 2.67%
DWTshear(223111)	28.47	29.19	29.91	30.37	30.91
DWTshear(416100)	28.52	29.25	29.82	30.17	30.68
HDWT	26.91	27.11	27.49	27.67	27.87
CSCT	26.89	27.33	27.92	28.28	28.67
NUDFB	28.06	28.90	29.16	29.21	29.46
CShear	28.22	28.54	28.82	29.41	29.70
DWT	27.77	28.52	29.13	29.61	30.07
QDWTshear	27.37	27.93	28.25	28.69	28.96
HQDWT	27.32	28.00	28.43	28.74	29.08
QNUDFB	27.99	28.49	28.98	29.40	29.87
QDWT	27.56	27.61	28.18	28.56	28.91
Shearlet	27.15	27.73	28.17	28.52	28.85

TABLE III
PSNR VALUES OF THE NLA FOR THE BARBARA IMAGE-5 LEVELS.

Num. of coeff.	5225 1.99%	5669 2.16%	6113 2.33%	6557 2.50%	7000 2.67%
DWTshear(223111)	26.47	26.85	27.14	27.33	27.79
DWTshear(333312)	27.00	27.17	27.41	27.53	27.70
HDWT	26.18	26.26	26.42	26.63	26.78
CSCT	25.90	26.11	26.32	26.53	26.74
NUDFB	25.58	25.77	25.99	26.08	26.24
CShear	25.55	25.68	25.80	25.99	26.04
DWT	25.36	25.58	25.72	25.92	26.11
QDWTshear	25.28	25.65	25.88	26.13	26.37
HQDWT	25.70	25.97	26.16	25.96	25.96
QNUDFB	24.90	24.62	24.91	25.19	25.58
QDWT	24.06	24.13	24.29	24.52	24.70
Shearlet	24.79	25.06	25.38	25.46	25.76

TABLE IV
PSNR VALUES OF THE NLA FOR THE LENNA IMAGE.

Num. of coeff.	17000 1.62%	19100 1.82%	21200 2.02%	23300 2.22%	25400 2.42%
DWTshear(223111)	30.56	32.91	34.44	35.47	36.25
DWTshear(414113)	30.56	32.91	34.45	35.47	36.26
HDWT	28.39	29.40	30.02	30.42	30.85
CSCT	29.61	31.57	32.67	33.67	34.30
NUDFB	30.35	32.09	33.52	33.83	34.23
CShear	30.35	32.30	33.16	33.70	34.40
DWT	29.97	32.12	33.73	34.57	35.42
QDWTshear	29.97	32.53	33.28	34.05	34.88
HQDWT	29.70	31.85	32.64	33.47	34.26
QNUDFB	30.26	32.22	33.49	34.34	35.00
QDWT	29.67	31.73	32.86	33.76	34.52
Shearlet	29.89	31.92	33.09	33.94	34.28

energy among the coefficients remains the same, in the finite domain setting, the NLA rate of a composite wavelet will eventually intersect and cross the NLA rate of a DWT or another critically sampled transform. These experiments succeed in demonstrating that these competitive transforms fail to have NLA rates that decay as rapidly as does DWTShear(223111) or the adaptive variant.

We also tested the performance of the Embedded Zerotree Wavelet (EZW) [33] and the Set Partitioning in Hierarchal Trees (SPIHT) [34] coding algorithms when combined with DWTShear transform on the *Barbara* and *Lenna* image. A 5-level decomposition was used for the DWT, the DWTShear, and the HDWT. The results are reported in Tables IX and X. Illustrations are shown in Figure 13. In addition, Figure 14 shows the difference in performance between DWTShear and DWT using the SPHIT encoder as a function of bit per pixel rate.

Whereas we do not consider these coding techniques as optimized to take full advantage of the structure inherent in DWTShear, it clearly indicates the possibility that many current wavelet-based compression routines might benefit greatly with a simple adjustment to the DWTShear structure and could be easily integrated in many of today's state-of-the-art compression schemes. It is expected that when many new coding schemes that exploit the NLA rate or more accurate parent-children relations are incorporated, even more significant improvements will be possible. We leave this development for future work.

V. CONCLUSION

In this paper, we have shown that the framework of wavelets with composite dilations provides a very flexible tool to: 1) analyze and generalize a number of oriented transforms that recently appeared in the literature; 2) construct new improved ones. Within this setting, we have derived some new critically sampled transforms and demonstrated their nonlinear approximation rate capabilities. Of particular value was the DWTShear construction that was demonstrated to efficiently represent a wide class of images and achieve excellent nonlinear approximation properties. In many cases, it achieves nearly 1 to 2 dB improvement over the DWT. A key observation over related transforms was not to strictly and

"blindly" enforce a parabolic scaling relation. It particular, an extremely simple adaptive variant was devised that could automatically determine the best angular partitioning with negligible overhead in structure calculation and description. Our results also show that the DWTShear transform can be used in combination with some of the well-known wavelet-based coding systems such as EZW and SPIHT to improve coding results. We envision that many current state-of-the-art wavelet-based coding schemes would greatly benefit without a significant computational overhead if the framework of the DWTShear were utilized to replace the standard DWT.

TABLE V
PSNR VALUES OF THE NLA FOR THE ZEBRA IMAGE.

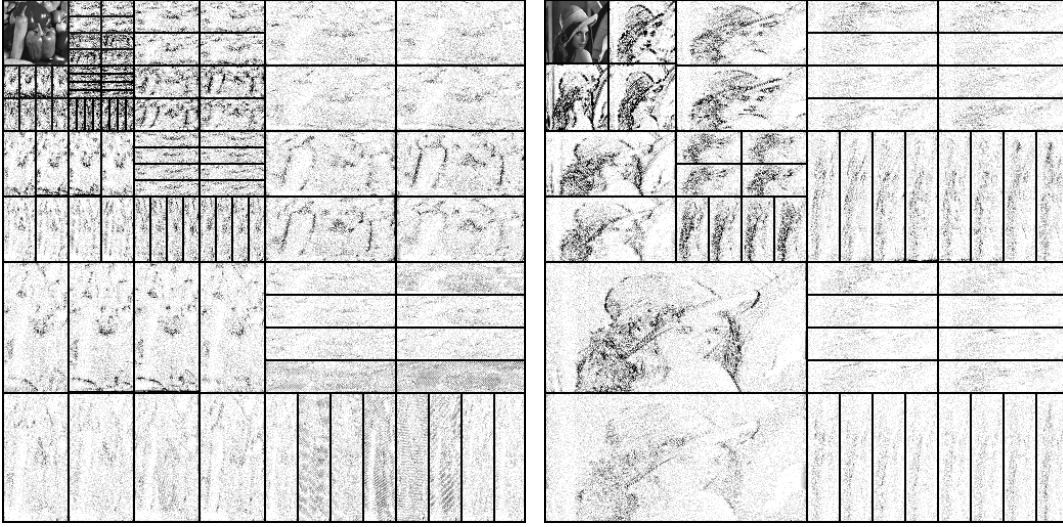| Num. of coeff.	3700 5.65%	4225 6.45%	4750 7.25%	5275 8.05%	5800 8.85%
DWTshear(223111)	23.66	24.17	24.52	24.94	25.41
DWTshear(320211)	23.71	24.20	24.87	25.29	25.85
HDWT	23.00	23.23	23.67	23.69	24.12
CSCT	22.38	22.68	23.12	23.53	23.83
NUDFB	22.24	22.47	22.73	22.87	23.34
CShear	23.02	22.54	22.82	23.24	23.28
DWT	23.12	23.61	24.06	24.54	24.95
QDWTshear	23.44	23.77	23.95	23.97	24.32
HQDWT	22.32	22.75	23.33	23.57	23.94
QNUDFB	22.61	23.20	23.61	23.96	24.26
QDWT	22.45	22.84	23.27	23.70	23.81
Shearlet	21.96	22.38	23.17	23.29	23.71

Fig. 9. Examples of the DWTShear decompositions of the *Peppers* image and the *Lenna* image. The image on the right is an example of the adaptive DWTShear decomposition of *Lenna*; its decomposition is succinctly described as DWTShear(414113).
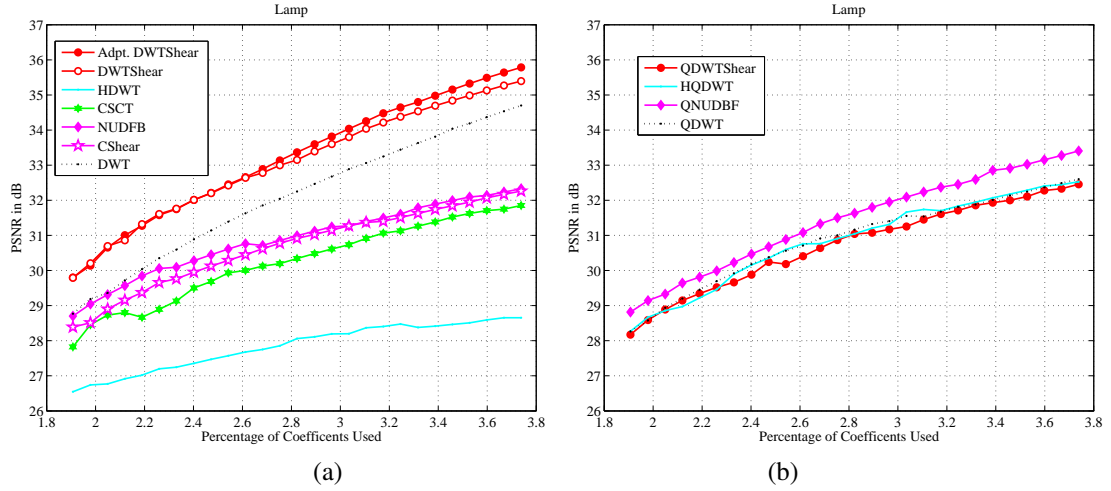

Fig. 10. Nonlinear approximation performance plots for *Lamp* image using $J = 3$. (a) Non-quincunx-based transforms. (b) Quincunx-based transforms.
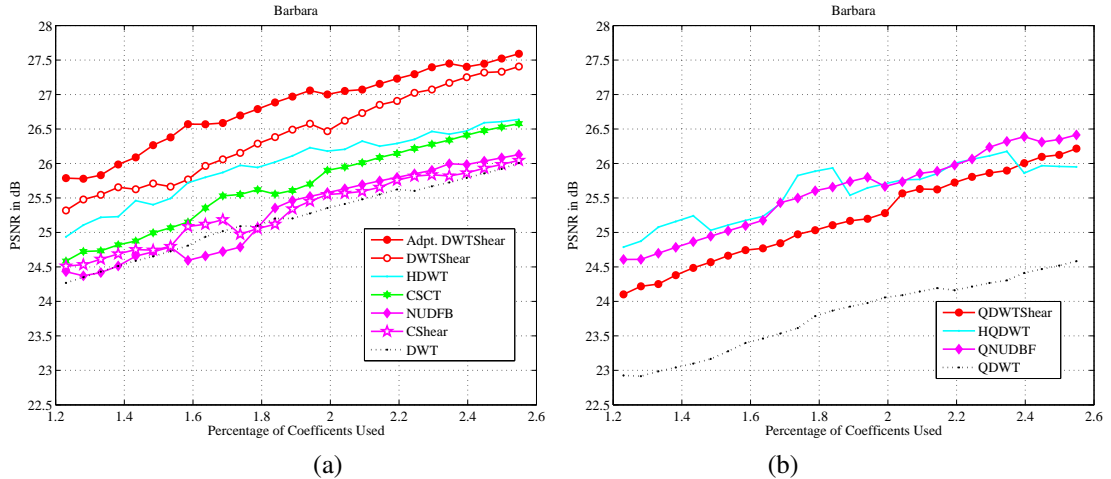

Fig. 11. Nonlinear approximation performance plots for *Barbara* image using $J = 5$. (a) Non-quincunx-based transforms. (b) Quincunx-based transforms.
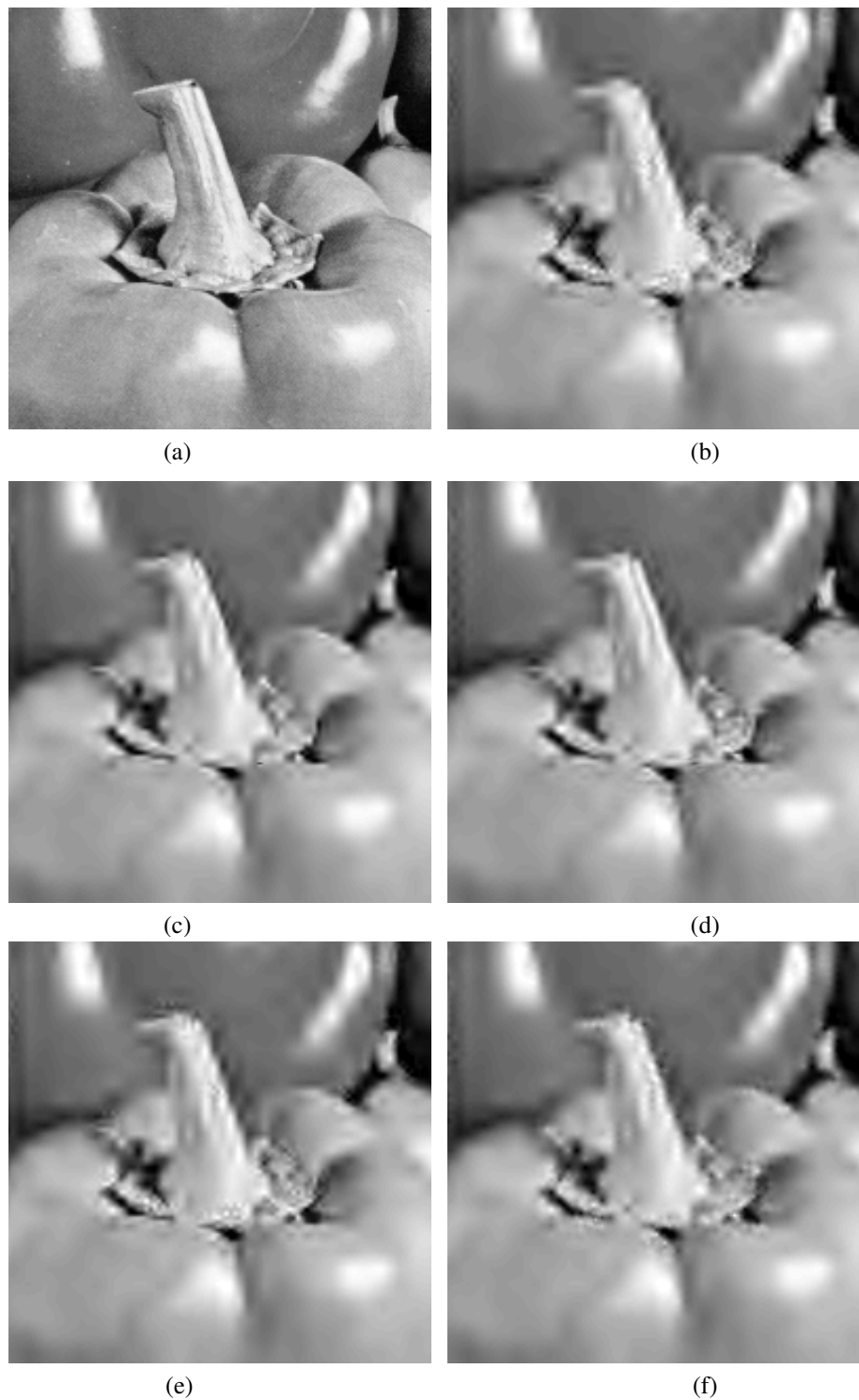
Fig. 12. Details of the nonlinear approximations using 5225 coefficients (1.99% of total number of coefficients) with the *Peppers* image. (a) Original image. (b) CShear (PSNR=28.22 dB). (c) DWT (PSNR=27.77 dB). (d) DWTShear(223111) (PSNR=28.47 dB). (e) NUDFB (PSNR=28.06 dB). (f) QNUDFB (PSNR=27.99 dB).
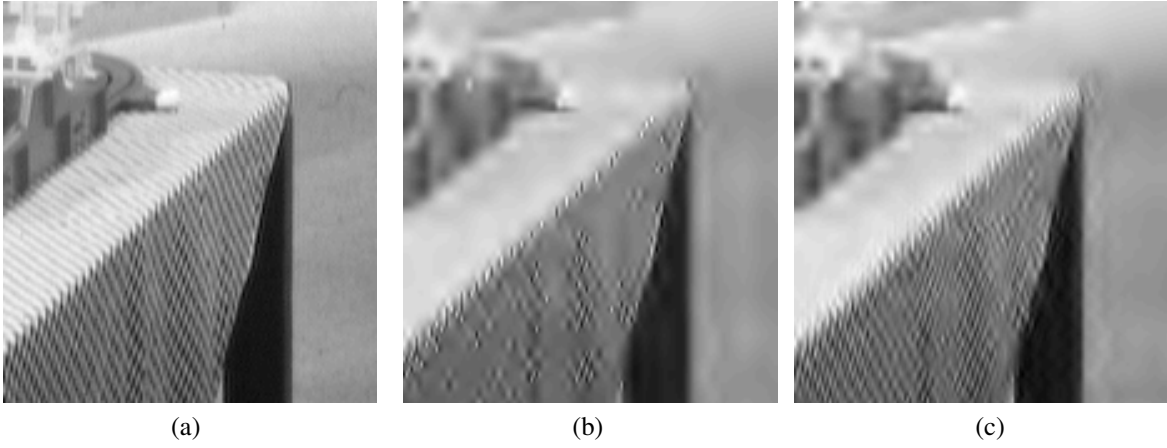
(a) (b) (c)

Fig. 13. Close-up images of coding results using the SPIHT algorithm for *Barbara* image at rate of 0.22 bpp. (a) Original image. (b) DWT (PSNR=26.99 dB). (c) DWTShear(223111) (PSNR=28.10 dB).

TABLE VI
PSNR VALUES OF THE NLA FOR THE CAT IMAGE -5 LEVELS.

Num. of coeff.	4195 0.10%	5244 0.13%	6292 0.15%	7341 0.18%	8389 0.20%
DWTshear(223111)	27.48	30.82	32.27	33.13	34.02
DWTshear(160161)	28.64	31.73	33.34	34.25	35.11
HDWT	25.70	27.32	28.11	28.57	28.91
CSCT	26.25	29.62	30.88	32.02	32.71
NUDFB	26.22	29.55	31.52	32.58	33.38
CShear	26.22	29.55	31.20	32.19	32.97
DWT	26.25	28.78	29.98	31.06	32.26
QDWTshear	27.32	29.06	30.55	31.31	32.03
HQDWT	27.32	29.69	31.03	31.73	31.96
QNUDFB	26.16	28.96	30.96	32.13	33.31
QDWT	27.32	28.86	29.90	30.59	31.55
Shearlet	26.10	28.46	29.57	30.53	31.11

TABLE VIII
PSNR VALUES OF THE NLA FOR THE LAMP IMAGE- 5 LEVELS.

Num. of coeff.	1300 1.98%	1563 2.38%	1825 2.78%	2088 3.19%	2350 3.59%
DWTshear(223111)	32.74	33.89	34.60	35.36	36.07
DWTshear(010010)	32.84	33.97	34.90	35.71	36.46
HDWT	27.69	28.13	28.34	28.62	28.78
CSCT	30.10	30.79	31.33	31.92	32.36
NUDFB	30.57	31.15	31.84	32.28	32.74
CShear	30.51	31.04	31.68	32.25	32.66
DWT	31.72	32.76	33.75	34.63	35.36
QDWTshear	30.30	30.91	31.65	32.24	32.75
HQDWT	30.49	31.43	31.87	32.39	32.95
QNUDFB	29.16	30.42	31.55	32.39	33.13
QDWT	30.50	31.23	31.69	32.37	32.97
Shearlet	29.19	30.05	30.81	31.54	32.12

TABLE VII
PSNR VALUES OF THE NLA FOR THE LAMP IMAGE.

Num. of coeff.	1007 1.54%	1268 1.93%	1529 2.33%	1790 2.73%	2050 3.13%
DWTshear(223111)	24.25	29.95	31.77	32.94	34.10
DWTshear(010010)	24.25	29.88	31.76	33.02	34.31
HDWT	23.90	26.63	27.25	27.79	28.40
CSCT	23.86	28.24	29.30	30.19	30.97
NUDFB	24.14	28.85	30.10	30.81	31.42
CShear	24.14	28.50	29.77	30.72	31.33
DWT	23.86	28.89	30.61	31.98	33.12
QDWTshear	24.62	28.34	29.67	30.81	31.45
HQDWT	23.66	28.40	29.91	30.87	31.78
QNUDFB	23.71	28.95	30.24	31.45	32.28
QDWT	24.62	28.39	29.93	30.98	31.58
Shearlet	23.86	28.01	29.55	30.46	31.34

Fig. 14. PSNR versus bit per pixel rate for the *Barbara* image using $J = 5$ for DWTShear(223111).

REFERENCES

[1] Bamberger R. H., and M. J. T. Smith, "A filter bank for directional decomposition of images: theory and design", *IEEE Trans. Signal Process.* , vol. 40, pp. 882–893, 1992.

[2] W. T. Freeman and E. H. Adelson, "The Design and Use of Steerable Filters", *IEEE Trans. Patt. Anal. Mach. Intell.*, vol. 13, no. 9, pp. 891–906, September 1991.

[3] E. P. Simoncelli and E. H. Adelson, "Non-separable Extensions of Quadrature Mirror Filters to Multiple Dimensions", *Proceedings of the IEEE*, vol. 78, no. 4, pp. 652–664, April 1990.

[4] Pietro Perona, "Steerable-scalable kernels for edge detection and junction analysis", in *2nd European Conf. Computer Vision*, pp. 3–18, 1992.

TABLE IX
PSNR VALUES FOR CODING USING BARBARA IMAGE.

BPP	coder	0.125	0.25	0.50	0.75	1.00
DWTShear(223111)	EZW	23.54	25.26	28.38	30.89	32.11
DWTShear(333312)	EZW	23.84	25.65	28.48	30.82	32.12
DWTShear(222111)	EZW	23.54	25.26	28.37	30.88	32.09
HDWT	EZW	22.98	25.10	27.83	29.91	31.24
DWT	EZW	23.00	24.29	27.23	30.20	31.39
DWTShear(223111)	SPIHT	25.55	28.39	32.02	34.58	36.54
DWTShear(333312)	SPIHT	25.89	28.44	31.90	34.46	36.42
DWTShear(222111)	SPIHT	25.55	28.40	32.03	34.60	36.55
HDWT	SPIHT	25.43	27.87	31.05	33.25	35.55
DWT	SPIHT	24.67	27.39	31.38	34.20	36.55

TABLE X
PSNR VALUES FOR CODING USING LENA IMAGE.

BPP	coder	0.125	0.25	0.50	0.75	1.00
DWTShear(223111)	EZW	32.42	35.69	39.00	41.90	42.51
DWTShear(414113)	EZW	32.43	35.69	39.01	41.91	42.54
DWTShear(222111)	EZW	32.42	35.69	39.00	41.90	42.51
HDWT	EZW	31.12	34.84	38.20	40.14	41.85
DWT	EZW	31.69	35.44	38.82	41.61	42.24
DWTShear(223111)	SPIHT	36.70	39.80	43.30	45.64	48.07
DWTShear(414113)	SPIHT	36.70	39.79	43.32	45.74	48.17
DWTShear(222111)	SPIHT	36.70	39.80	43.30	45.64	48.07
HDWT	SPIHT	35.80	38.81	42.35	44.80	47.26
DWT	SPIHT	36.37	39.67	43.10	45.34	47.50

[5] J L Starck, E J Candès and DL Donoho, "The Curvelet Transform for Image Denoising", *IEEE Trans Image Process.*, vol. 11, pp. 670–684, 2000.

[6] M. N. Do, and M. Vetterli, "The contourlet transform: an efficient directional multiresolution image representation", *IEEE Trans. Image Process.*, vol. 14, no. 12, pp. 2091–2106, Dec. 2005.

[7] K. Guo, W.-Q Lim, D. Labate, G. Weiss and E. Wilson, "Wavelets with composite dilations", *Electron. Res. Announc. Amer. Math. Soc.*, vol. 10, pp. 78–87, 2004.

[8] E. J. Candès and D. L. Donoho, "New tight frames of curvelets and optimal representations of objects with piecewise C^2 singularities", *Comm. Pure and Appl. Math.*, vol. 56, pp. 216–266, 2004.

[9] K. Guo and D. Labate, "Optimally sparse multidimensional representation using shearlets", *SIAM J. Math. Anal.*, vol. 9, pp. 298–318, 2007.

[10] G. Easley, W. Lim, and D. Labate, "Sparse Directional Image Representations using the Discrete Shearlet Transform", *Appl. Comput. Harmon. Anal.*, vol. 25, pp. 25–46, 2008.

[11] D. D. Po and M. N. Do, "Directional multiscale modeling of images using the contourlet transform," *IEEE Trans. Image Process.*, vol. 15, no. 6, pp. 1610–1620, June 2006.

[12] S. Yi, D. Labate, G. R. Easley, and H. Krim, "A Shearlet approach to Edge Analysis and Detection", *IEEE Trans. Image Process.*, vol. 18, no. 5, pp. 929–941, 2009.

[13] R. Eslami, H. Radha, "New image transforms using hybrid wavelets and directional filter banks: Analysis and design", *Proc. IEEE Int. Conf. Image Process. ICIP2005.* Genova, Italy, Sept. 2005.

[14] R. Eslami and H. Radha, "Regular hybrid wavelets and directional filter banks: Extensions and applications", *Proc. IEEE Int. Conf. Image Process. ICIP2006.* Atlanta, GA, Oct. 2006.

[15] R. Eslami, H. Radha, "A New Family of Nonredundant Transforms Using Hybrid Wavelets and Directional Filter Banks", *IEEE Trans. Image Process.*, vol. 16, no. 4, pp. 1152–1167, April 2007.

[16] S. Higaki, S. Kyochi, Y. Tanaka, and M. Ikehara, "A novel design of critically sampled contourlet transform and its application to image coding", *Proc. IEEE Int. Conf. Image Process. ICIP2008.* San Diego, CA, Oct. 2008.

[17] Y. Tanaka, M. Ikehara, and T Q Nguyen, "Multiresolution Image Representation using Combined 2D and 1D Directional Filter Banks", *IEEE Trans. Image Process.*, vol. 18(2), pp. 269-280, Feb. 2009.

[18] E. LePennec and S. Mallat, "Sparse geometric image representation with bandelets", *IEEE Trans. Image Process.*, vol. 14, no. 4, pp. 423438, Apr. 2005.

[19] V. Velisavljevic, B. Beferull-Lozano, M. Vetterli, and P. L. Dragotti, "Directionlets: Anisotropic multidirectional representation with separable filtering", *IEEE Trans. Image Process.*, vol. 15, no. 7, pp. 19161933, Jul. 2001.

[20] F. C. A. Fernandes, R. L. C. van Spaendonck, and C. S. Burrus, "Multidimensional, mapping-based complex wavelet transforms", *IEEE Trans. Image Process.*, vol. 14, no. 1, pp. 110-124, Jan. 2005.

[21] K. Guo, W-Q. Lim, D. Labate, G. Weiss and E. Wilson, "Wavelets with composite dilations and their MRA properties", *Appl. Comput. Harmon. Anal.*, vol. 20, pp. 220–236, 2006.

[22] K. Guo, W-Q. Lim, D. Labate, G. Weiss and E. Wilson, "The theory of wavelets with composite dilations", in: Harmonic Analysis and Applications, C. Heil (ed.), pp. 231–249, Birkhäuser, Boston, MA, 2006.

[23] J. D. Blanchard, "Minimally supported frequency composite dilation wavelets", *J. Fourier Anal. Appl.*, vol. 15, pp. 796–815, 2009.

[24] J. D. Blanchard, "Minimally Supported Frequency Composite Dilation Parseval Frame Wavelets", *J. Geom. Anal.*, vol. 19, pp. 19–35, 2009.

[25] J. D. Blanchard and I. A. Krishtal, *Matricial filters and crystallographic composite dilation wavelets*, preprint, 2010.

[26] I. Kryshtal, B. Robinson, G. Weiss, and E. Wilson, "Compactly supported wavelets with composite dilations", *J. Geom. Anal.*, vol. 17, pp. 87–96, 2006.

[27] K. Guo, and D. Labate, "Characterization and analysis of edges using the continuous shearlet transform", pp. 29, to appear in SIAM on Imaging Sciences, 2009.

[28] G. Kutyniok, and D. Labate, "Resolution of the Wavefront Set using the Continuous Shearlet Transform", *Trans. AMS*, vol. 361, pp. 2719–2754, 2009.

[29] T. T. Nguyen and S. Oraintara, "Multiresolution direction filterbanks: Theory, design, and applications", *IEEE Trans. Signal Process.*, vol. 53, no. 10, pp. 3895-3905, Oct. 2005.

[30] S. Mallat, *A Wavelet Tour of Signal Processing*, Academic Press, San Diego, 1998.

[31] W-Q. Lim, "Wavelets with Composite Dilations," Ph.D. Thesis, Dept. Mathematics, Washington University in St. Louis, St. Louis, MO, 2006.

[32] F. Colonna, G. R. Easley, K. Guo, and D. Labate, "Radon Transform Inversion using the Shearlet Representation", *Appl. Comput. Harmon. Anal.*, vol. 29, no. 12, pp. 232–250, 2010.

[33] J. Shapiro, "Embedded image coding using zerotree of wavelet coefficients", *IEEE Trans. Signal Proc.*, vol. 41, no. 12, pp. 3445–3462, Dec. 1993.

[34] A. Said, and W. A. Pearlman, "A new fast and efficient image codec based on set partitioning in hierarchical trees", *IEEE Trans. Circuits Syst. Video Technol.*, vol. 6, no. 3, pp. 243-250, Jun. 1996.

Glenn R. Easley received the B.S. (with honors) and M.A. degrees in mathematics from the University of Maryland, College Park, in 1993 and 1996, respectively, and the Ph.D. degree in computational science and informatics from George Mason University in 2000. Since 2000, he has been with System Planning Corporation working in signal and image processing. He has also been a Visiting Assistant Professor for the Norbert Wiener Center, University of Maryland, since 2005. His research interests include computational harmonic analysis, with special emphasis on wavelet theory and time-frequency analysis, synthetic aperture radar, deconvolution, and computer vision.

Demetrio Labate received the Ph.D. degree in electrical engineering from the Politecnico di Torino, Italy, in 1995, and the Ph.D. degree in Mathematics from the Georgia Institute of Technology, Atlanta, in 2000. He was a Chauvenet lecturer at Washington University in St.Louis and later in the faculty at North Carolina State University. Since 2009, he is Associate Professor at the Department of Mathematics of the University of Houston. His research interests include harmonic analysis, wavelet theory, time-frequency analysis and sparse representations. Prof. Labate received the NSF CAREER Award in Applied Mathematics in 2008.